Biochimica et Biophysica Acta 1848 (2015) 1023–1031

Contents lists available at ScienceDirect

Biochimica et Biophysica Acta

journal homepage: www.elsevier.com/locate/bbamem

A novel fragment based strategy for membrane active antimicrobials against MRSA

Jianguo Li [a,b,g], Shouping Liu [a,g], Jun-Jie Koh [a,e], Hanxun Zou [a], Rajamani Lakshminarayanan [a], Yang Bai [a,c], Konstantin Pervushin [c], Lei Zhou [a], Chandra Verma [a,b,c,d,*], Roger W. Beuerman [a,e,f,g,**]

[a] Singapore Eye Research Institute, 11 Third Hospital Avenue, #06-00, 168751, Singapore
[b] Bioinformatics Institute (A*-STAR), 30 Biopolis Street, #07-01 Matrix, 138671, Singapore
[c] School of Biological Sciences, Nanyang Technological University, 60 Nanyang Drive, 637551, Singapore
[d] Department of Biological Sciences, National University of Singapore, 14 Science Drive 4, 117543, Singapore
[e] Department of Ophthalmology, Yong Loo Lin School of Medicine, National University of Singapore, 5 Lower Kent Ridge Road, 119074, Singapore
[f] School of Chemical and Biomedical Engineering, Nanyang Technological University, 62 Nanyang Drive, 637459, Singapore
[g] Duke-NUS, SRP Neuroscience-Behavioural Disorders, Singapore

ARTICLE INFO

Article history:
Received 29 September 2014
Received in revised form 29 December 2014
Accepted 5 January 2015
Available online 10 January 2015

Keywords:
Membrane active antimicrobials
Molecular dynamics simulations
Fragment based drug design
Pharmacophore model

ABSTRACT

Membrane active antimicrobials are a promising new generation of antibiotics that hold the potential to avert antibiotic resistance. However, poor understanding of the action mechanism and the lack of general design principles have impeded their development. Here we extend the concept of fragment based drug design and propose a pharmacophore model based on first principles for the design of membrane active antimicrobials against Gram positive pathogens. Elaborating on a natural xanthone-based hydrophobic scaffold, two derivatives of the pharmacophore model are proposed, and these demonstrate excellent antimicrobial activity. Rigorous molecular dynamics simulations combined with biophysical experiments suggest a three-step mechanism of action (absorption–translocation–disruption) which allows us to identify key factors for the practical optimization of each fragment of the pharmacophore. Moreover, the model matches the structures of several membrane active antimicrobials which are currently in clinical trials. Our model provides a novel and rational approach for the design of bactericidal molecules that target the bacterial membrane.

1. Introduction

Widespread antibiotic resistance has become a global healthcare problem [1,2]. Resistant pathogens have been readily found against every class of antibiotics, including vancomycin and the recently approved drugs such as linezolid and daptomycin. As a result, treatment of infections caused by resistant pathogens such as *vancomycin-resistant enterococcus* (VRE) and *methicillin-resistant Staphylococcus aureus* (MRSA) pose substantial challenges [3–5]. Membrane active antimicrobials [6] such as antimicrobial peptides (AMPs) [7,8] and synthetic peptidomimetics [9,10] may offer a potential solution to this problem, as these molecules act on the bacterial membrane, which is evolutionarily conserved and difficult for the bacteria to develop resistance. In contrast, commonly used antibiotics interfere with bacterial biosynthesis, centering on proteins which are easily mutated resulting in loss of recognition of the "docking site" by the antibiotic, thus rendering them ineffective. Compared with AMPs, synthetic peptidomimetics are commercially more promising due to their simple structures, lower costs and high stability. The development of rational principles for the design of membrane active peptidomimetics would stimulate this developing area [11].

The action mechanism of AMPs at the molecular level has been extensively studied experimentally and computationally in the past several decades and several modes of action have been proposed, namely, the barrel-stave model, the toroidal model and the carpet model [12–15]. However, few atomistic insights are available for the action mechanism of synthetic peptidomimetics, which has impeded their further development. In silico methods such as molecular docking [16], in principle, could provide atomic level information of molecular interactions, but these are largely limited to the design of traditional antibiotics. For the design of membrane active AMPs/peptidomimetics, molecular docking usually fails because of a poor understanding of the actual action mechanism, the lack of well-defined molecular cavities for drug binding in the membrane, the dynamic nature of the membranes due to their fluidity and the diverse binding modes of these molecules to the membrane. Instead, molecular dynamics (MD) simulations are now commonly being used to understand the detailed atomistic dynamics

* Correspondence to: C. Verma, Bioinformatics Institute (A*-STAR), 30 Biopolis Street, #07-01 Matrix, 138671, Singapore.
** Correspondence to: R.W. Beuerman, Singapore Eye Research Institute, 11 Third Hospital Avenue, #06-00, 168751, Singapore.
E-mail addresses: chandra@bii.a-star.edu.sg (C. Verma), rwbeuerman@gmail.com (R.W. Beuerman).

http://dx.doi.org/10.1016/j.bbamem.2015.01.001
0005-2736/

of such processes in the exploration of the mechanism of AMPs and peptidomimetics [12,14,17].

A number of simulation and experimental studies have shown that both hydrophobic and electrostatic interactions are important in the interactions of AMPs with the bacterial membrane [12,18,19]. This is because most AMPs are amphiphilic and can insert their hydrophobic moieties into the lipid tail region of the bacterial membrane, while their cationic groups interact with the anionic head groups. To mimic the amphiphilic structure of AMPs, based on different hydrophobic scaffolds, several synthetic peptidomimetics have been reported in the last decade. For example, using an arylamide scaffold, Tew et al. have designed a series of cationic antimicrobial foldamers, such as PMX-30016 and PMX-30063 to mimic the interaction of maganin with bacterial membranes [17]. Using porphyrin as a hydrophobic scaffold, Ooi et al. added two cationic groups and developed a new membrane active antimicrobial XF-73 with rapid bacterial killing and excellent antimicrobial activity [20]. Other hydrophobic scaffolds have also been used in the development of the membrane active peptidomimetics such as LTX-109 [21], CSA-13 [22] and BPMTAs [23]. Using a similar approach, our group selected alpha-mangostin, a naturally occurring xanthone isolated from the pericarp of the tropical fruit mangosteen as the hydrophobic scaffold because of its high membrane affinity [24]. We modified this scaffold by adding two cationic groups and obtained a series of amphiphilic xanthone analogues [25]. One of the xanthone analogues AM0016 (Fig. 1) showed excellent antimicrobial activity and rapid killing kinetics, demonstrating great potential for further structural optimization.

Microbial killing by membrane active antimicrobials is a complex process. For Gram positive pathogens such as MRSA, the disruption of the inner membrane is usually the rate limiting step [6], while for Gram negative pathogens, the thick outer membrane made up of lipopolysaccharide (LPS) molecules is a significant barrier to most antimicrobial molecules and permeation through such barriers is most likely a critical rate limiting step [26–28]. In this study, our goal is to develop practical principles for the design of new antimicrobials against Gram positive pathogens, particularly MRSA; therefore we focus only on the bacterial inner membrane. From a structural point of view, the bacterial inner membrane can be decomposed into three fragments: two anionic head group regions and one hydrophobic region, and it is this decomposition that provides the basis for the development of a fragment based strategy [29] (Fig. 1). We hypothesize that a molecule that perturbs all three fragments of the bacterial inner membrane will likely have high membrane activity. As such, we propose a bola-like pharmacophore model that consists of two cationic arms and one hydrophobic scaffold, which complementarily interact with the two anionic head group fragments and the lipid tail fragment, respectively. The hydrophobic scaffold provides affinity for the lipid tails of the bacterial membrane, while the two cationic groups preferentially interact with the two anionic head group regions of the bacterial membrane. One can deduce from the model that upon initial adsorption on the surface of the bacterial outer leaflet, the molecule would adopt a U-shaped conformation, with both cationic groups interacting with the head groups of the outer leaflet and the hydrophobic scaffold embedded in the lipid tail region. To achieve a transmembrane conformation, one of the cationic groups needs to translocate across the lipid tail region of the membrane, which, at first glance appears energetically prohibitive and hence unlikely; however, we find that this indeed is possible, albeit at high drug concentrations, as we will demonstrate below.

In this study, we employ a multi-disciplinary approach which involves MD simulations, biophysical and microbiological experiments to decipher the detailed action mechanism of the pharmacophore model using AM0016 as a model compound (Fig. 1). First we vary the structure of the hydrophobic scaffold and the cationic groups of AM0016 to examine the role of each fragment using MD simulations. The resulting new analogues are synthesized and validated using biophysical and microbiological experiments. Finally we discuss some principles for the practical design of active bolaamphiphilic molecules against bacterial membranes.

2. Results

2.1. Role of the hydrophobic scaffold

In the pharmacophore model, the role of the hydrophobic scaffold is to drive the molecule deeply into the hydrophobic region of the membrane followed by translocation. Hydrophobic scaffolds with high affinity for the lipid tails are likely to partition more into the membrane, i.e., have high interfacial activity [30]. This is an energetically favourable step and requires the identification of a proper hydrophobic scaffold that most optimally embeds into the membrane. Alpha-mangostin has been demonstrated, through our development of AM0016 [24,25], to be an appropriate scaffold. Two structural properties, notably the planarity and the hydrophobicity of the scaffold favour its penetration into the hydrophobic region of the bacterial membrane. However, high hydrophobicity of a molecule is believed to lead to high toxicity to human membranes [31–33]. Thus it is important to estimate the optimum hydrophobicity of the scaffold required to maintain the affinity for the lipid tails of the bacterial membrane. As shown in Fig. 2a, the

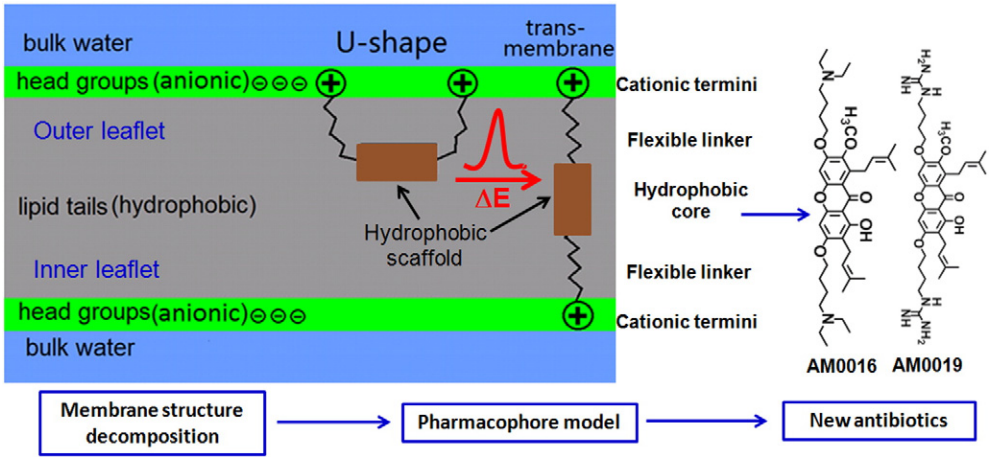

Fig. 1. The schematic view of the xanthone based pharmacophore model containing five fragments: alpha-mangostin as the hydrophobic core, two cationic terminal groups and two flexible linkers. The bacterial membrane contains a high percentage of anionic lipids. Initially the molecule gets adsorbed with U-shaped conformations; at high surface concentrations, the molecule overcomes an energy barrier and undergoes a conformational change, resulting in a trans-membrane conformation, which can induce larger membrane perturbations than the U-shaped conformation. AM0016 and AM0019 are the two derivatives of the pharmacophore model.

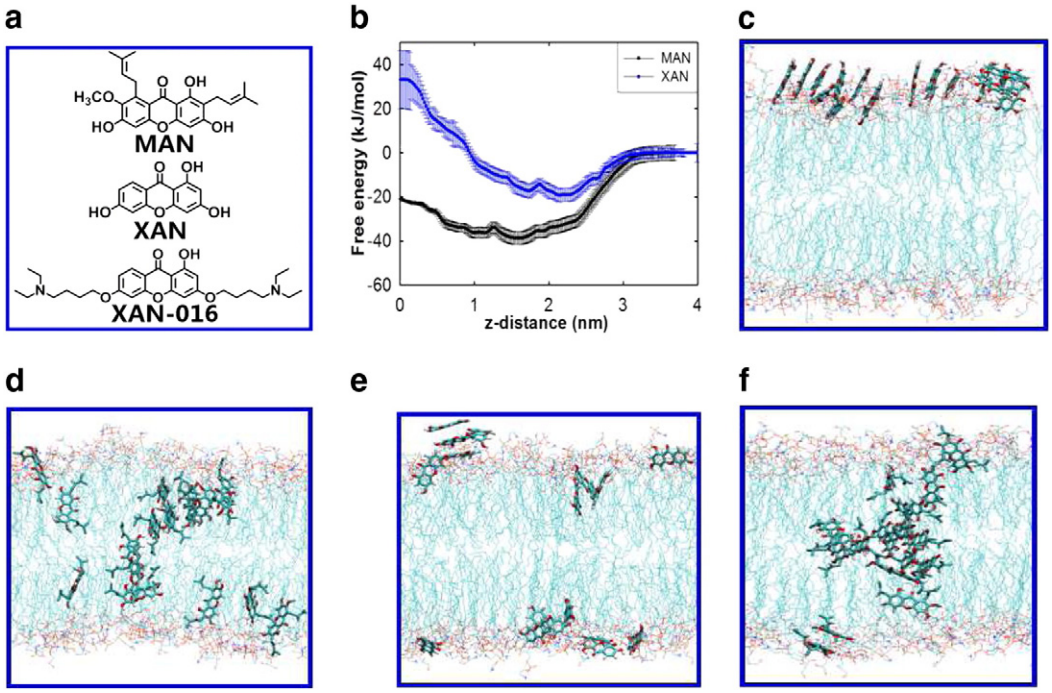

Fig. 2. (a) Chemical structures of MAN, XAN and XAN-016; (b) transfer free energies of alpha-mangostin (MAN) and xanthone analogue without the isoprenyl groups (XAN) from solvent; (c) configuration of 16 XAN molecules on the bacterial membrane with 16 XAN molecules initially put on top of the bacterial membrane; (d) configuration of 16 MAN molecules on the bacterial membrane with the 16 MAN molecules initially put on top of the bacterial membrane; (e) configuration of 16 XAN molecules on the bacterial membrane with the 16 XAN molecules initially put at the centre of the bacterial membrane; (f) configuration of 16 MAN molecules on the bacterial membrane with the 16 MAN molecules initially put at the centre of the bacterial membrane.

two isoprenyl groups contributed significantly to the overall hydrophobicity of alpha-mangostin [24], and hence it is important to explore whether the xanthone analogue with the isoprenyl group removed could still maintain the affinity for the lipid tail region of the bacterial membrane. To such purpose, we first compared the affinities of alpha-mangostin (referred to as MAN hereafter) and the analogue with isoprenyl groups removed (referred to as XAN) for the bacterial membrane using MD simulations.

To estimate the ability of these two molecules to partition into the membrane, we calculated their transfer free energies from solvent using umbrella sampling and the weighted histogram analysis method [34] (Fig. 2b). It is clear that MAN encounters lower transfer free energies than XAN and hence can penetrate more easily into the bacterial membrane. This suggests that the two isoprenyl groups contribute significantly to the affinity of alpha-mangostin for the lipid tail region of the bacterial membrane. In contrast, in the absence of the isoprenyl groups, the hydrophobicity is attenuated by the polar groups in the aromatic rings, resulting in the loss of affinity of XAN for the lipid tails. The transfer free energies of MAN and XAN were calculated using a single molecule, which corresponds to a low compound/lipid ratio. High compound/lipid ratios were explored by carrying out microsecond long conventional MD simulations at a compound/lipid ratio of 16/128 for both molecules. Fig. 2c and d show that at a higher concentration, MAN can penetrate and accumulate in the lipid tail region of the bacterial membrane, while XAN prefers to remain on the surface of the bacterial membrane, consistent with the free energy results. It is of course possible that XAN may penetrate at longer simulation times. To examine this, we ran a separate simulation with 16 MAN or 16 XAN molecules initially placed in the lipid tail region of the bacterial membrane. At the end of the simulation, most of the MAN molecules remained in the lipid tail region of the bacterial membrane, while none of the XAN molecules remained deeply embedded in the lipid tail region (Fig. 2e and f). Among the 16 XAN molecules, 11 moved out of the bacterial membrane on to the membrane surface. The remaining 5 XAN molecules moved close to the membrane surface, remaining just beneath the head groups. The inability of XAN to partition sufficiently into the lipid tail region of the bacterial membrane indicates that the two isoprenyl groups serve as membrane probes and thus are a critical component of the xanthone scaffold.

To validate the importance of the isoprenyl group, we synthesized a new compound XAN-016, with the isoprenyl group removed from AM0016 (Fig. 2a). An in vitro antimicrobial test showed little or no activity of XAN-016 against various *Staphylococcus aureus* strains including MRSA, with minimum inhibitory concentrations (MIC) above 50 μg/mL (Table 1), consistent with the observations made from the simulation. Based on the simulation and experimental results, we retained the isoprenyl groups on the xanthone scaffold of the pharmacophore model and next examined the role of the cationic groups.

2.2. Role of the terminal cationic groups

The main difference between the physicochemical characteristics of the bacterial membrane and the mammalian membrane lies in their head groups, with the former being anionic and the latter zwitterionic. The cationic fragments of the pharmacophore model can selectively interact with the anionic head groups via electrostatic interactions and thus can be critical for antimicrobial activity as well as for selectivity. We have previously found that cationic groups with high pKa values and low hydrophobicity are essential for antimicrobial activity as well as selectivity [25]. To further explore the selectivity, we mutated the diethylamide group (pKa 10.95) of AM0016 to guanidinium (pKa 12.48), creating a new compound AM0019 (Figs. 1 and S1). We further hypothesized that the lower hydrophobicity of the guanidinium group may also result in reduced toxicity of AM0019 against mammalian membranes.

The affinities of the two analogues (AM0016 and AM0019) for a model bacterial membrane were estimated by calculating their transfer free energies from solvent. As illustrated in our model, the cationic group of the drug molecule needs to overcome a free energy barrier

Table 1
Minimum inhibitory concentrations ([a]MIC) of xanthone analogues (μg/mL).

	Description	XAN-016	AM0016	AM0019
MRSA 9808R	*Methicillin-resistant staphylococcus aureus* (+)[b]	>50	1.56	6.25
SA DM 4001R	Clinical isolates *Staphylococcus aureus* (+)	>50	1.56	3.125
MRSA 21455	*Methicillin-resistant staphylococcus aureus* (+)	>50	0.39	6.25
BC 11778	*Bacillus cereus* (+)	>50	3.125	6.25
PA DM23155	Clinical isolates *Pseudomonas aeruginosa* (−)[c]	>50	>25	>25
Kleb DM4299	Clinical isolates *Klebsiella pneumonia* (−)	>50	>25	>25

[a] The MIC is repeated two time for each assay, and the standard deviation is +/− 1x MIC.
[b] (+) denotes Gram positive strain.
[c] (−) denotes Gram negative strain.

when crossing the hydrophobic region of the membrane, facilitated by a conformational change from the U-shape to the transmembrane conformations (Fig. 3a). This conformational change depends on the inherent deformability of the membrane and other 'hidden' degrees of freedom, and may lead to hysteresis during the computation if the centre of mass is pulled in the forward and reverse directions. As the free energy barrier arises mainly from the introduction of the cationic group in the lipid tail region, we chose the distance between one of the cationic groups and the bilayer centre as the reaction coordinate. As shown in Fig. 3b, both AM0016 and AM0019 show qualitatively similar trends in their translocation free energies, indicating similar modes of actions. The two free energy minima, located at 2 nm and −1 nm, correspond to the U-shaped and the transmembrane conformations, respectively, while the free energy barrier corresponds to the transition state that characterizes the crossing of the hydrophobic region of the membrane by the cationic group (Fig. 3a). However, the free energy profiles of the two molecules are quantitatively different. AM0019 shows a higher free energy barrier than AM0016 at the transition state because the guanindine group of AM0019 is less hydrophobic than the diethalamine group of AM0016. Moreover, the high hydrophobicity of diethalamine group also incurs less desolvation costs when adsorbed on the surface of the bacterial membrane, as seen from the more favourable free energy minimum of AM0016 in its U-shaped conformation (around 2 nm).

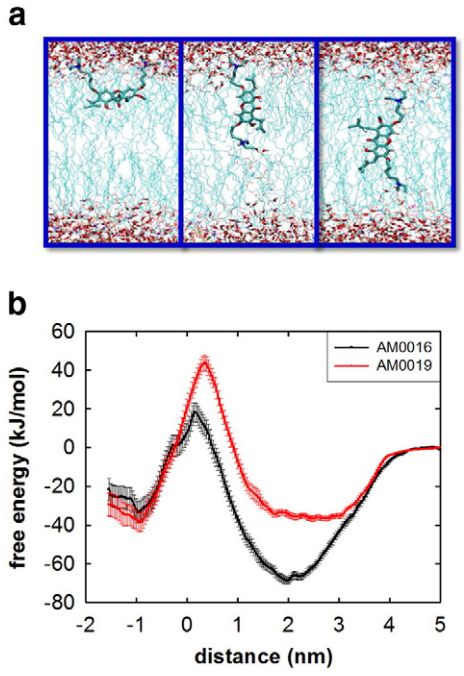

Fig. 3. (a) Snapshots showing the conformational change of AM0016 during penetration into the bacterial membrane. (b) Transfer free energy of AM0016 and AM0019 across the bacterial membrane as a function of the distance between one cationic group and the bilayer centre.

In summary, the above simulation results reveal two possible conformations of AM0016 and AM0019 occurring sequentially—first the U-shaped and then the transmembrane conformations.

The high free energy barrier for the conformational change is obtained using one molecule of AM0016 or AM0019 and 72 molecules of lipids, corresponding to a low drug concentration. As the surface concentration of AM0016/AM0019 on the outer leaflet increases, the anionic charges of the outer leaflet will gradually be neutralized. This will result in an asymmetry of charges experienced by the cationic sidechains, with a strong electrostatic pull towards the inner leaflet which does not experience charge neutralization. Consequently, the local minimum seen at around 2 nm will become shallow and the free energy barrier will be much lower. In addition, as more molecules get adsorbed on the outer leaflet, the membrane undergoes significant perturbations, which further lowers the free energy barrier, making the translocation of the cationic group much easier. This is similar to the conformational change seen for cationic bolaamphiphilic molecules when they interact with membranes consisting of anionic lipids [35]. In fact, it appears that some AMPs also follow a similar mode of action. At low concentrations some AMPs such as magainin 2, MSI-78, melittin and alamethicin lie parallel to the outer leaflet, while at high concentrations they were found to penetrate into the membrane and span it, resulting in the formation of transmembrane pores [36–40]. Moreover, even bulky cationic dendrimers such as PAMAM have been reported to locate at the membrane surface at low concentrations, but to penetrate into and span the zitterionic bilayer in a transmembrane conformation at high concentrations [41]. Considering the smaller size of the AM0016/AM0019 molecule and the electrostatic interactions between the cationic groups of AM0016/AM0019 and the anionic head groups of the bacterial membrane, it is likely that some AM0016/AM0019 molecules may undergo conformational changes and assume extended conformations when the drug/lipid ratio is high. It is also possible that some AM0016/AM0019 molecules will further translocate across the bacterial membrane, adopting the U-shaped conformation at the inner leaflet. Hence, at high drug concentrations, both the U-shaped and the extended conformations likely co-exist, perturbing both leaflets of the bacterial membrane. The results suggest that to induce sufficient membrane perturbations, a critical drug/lipid ratio exists, consistent with the experimental observation that a minimum inhibitory concentration (MIC) is required for microbial killing. We next examine the effects of increasing concentrations of AM0016/AM0019.

2.3. High concentration of AM0016/AM0019 induces significant membrane perturbations

In their transmembrane conformations, both AM0016 and AM0019 interact simultaneously with the three fragments of the bacterial membrane and this is expected to induce more significant membrane perturbations than would result from the U-shaped conformations. However, the transmembrane conformation occurs at high drug/lipid ratios, such as in the case of microbiological killing assays. In contrast, stoichiometric analysis showed that most biophysical experiments (e.g., dye-leakage experiment, NMR) were performed at drug/lipid

ratios that are several orders lower than typical in bacterial killing assays [30]. Moreover, the transmembrane conformation likely leads to membrane instability and disruption. Therefore it is difficult to probe the transmembrane conformations through biophysical experiments. Instead, molecular dynamics simulations provide an ideal tool to explore such features.

In order to understand how the transmembrane conformation affects membrane integrity, we performed microsecond long molecular dynamics simulations using 4, and 16 molecules of AM0016 and AM0019 embedded in a membrane patch of 128 lipids, reflecting respectively low and high concentrations of AM0016 and AM0019. The density profiles of phosphate atoms in Fig. S2 suggest significant membrane perturbations when the AM0016/AM0019 concentration becomes high. This leads to significant membrane deformation and the formation of lipid defects filled with water molecules at high AM0016/AM0019 concentrations (Fig. S3). As a result, a large number of water molecules were found to translocate across the membrane, indicating that the membrane becomes leaky. AM0019 induces little larger membrane deformations than AM0016, which may arise from the bidentate hydrogen bonds formed between the guanidine groups of AM0019 and the PO_4 groups of lipid molecules. To understand the interactions of the cationic groups with the phosphate groups, we calculated the radial distribution function between the centre of mass of the cationic groups of AM0016/AM0019 and the centre of mass of the PO_4 groups of the lipid molecules. As expected, AM0019 shows a much higher peak than AM0016, indicating that the guanidinium group has stronger interactions with PO_4 groups than does the diethalamine group (Fig. S4). In addition, the apparent area per lipid (AAPL, defined as the area of the simulation box in the xy plane divided by the number of lipid molecules in each leaflet) increases with the AM0016/lipid ratio. At the highest AM0016/lipid ratio (16/128), the AAPL increased almost 40% with respect to that of a pure bacterial membrane (Fig. S5). However, in the presence of 16 AM0019 molecules, the membrane is significantly distorted (Fig. S3), resulting in only a slight increase in AAPL. Apart from the perturbations in the membrane structure, both AM0016 and AM0019 were found to aggregate in the membrane, forming 2-D clusters in which the central hydrophobic cores stacked together in the hydrophobic region of the bilayer with the two cationic groups located at the head group regions of the two leaflets (Fig. 4a and b). This is associated with a re-distribution of the lipids and the formation of raft-like domains that are rich in anionic lipids (e.g., POPG) around the cationic AM0016/AM0019 clusters. These are driven by electrostatics and significantly affect the integrity and the mechanical properties of the bacterial membrane. In particular, the pressure field [42] of the bacterial membrane was found to change only a little at a low AM0016/AM0019 concentration, but significantly at a high AM0016/AM0019 concentration (Fig. 4c), with the disappearance of the two negative peaks. This suggests that the hydrophobic-water interface is destabilized and is accompanied by a drastic change in the elastic properties of the bacterial membrane [43].

Our simulation results predict that AM0019 is membrane active and induces membrane perturbations similar to those of AM0016. To validate the observations from the simulations, we synthesized AM0019 (Fig. S1) and examined membrane leakage using both biophysical and microbiological experiments. The induced dye-leakage (Fig. 5) and the MIC value (Table 1) demonstrate that both AM0016 and AM0019 are membrane active, consistent with our simulation predictions. In the dye-leakage experiment, AM0019 was found to have slightly larger inner membrane activity, as revealed by the larger membrane leakage of AM0019 (Figs. 5a and S6). However, in the microbiological killing assays, the antimicrobial activity of AM0019 was shown to be slightly weaker than that of AM0016 (Table 1). Notice that in the dye-leakage experiment which uses unilamellar vesicles (LUV), the drug molecules directly target the membrane, while in the bacterial killing assays, before targeting the inner membranes, the molecules need to permeate through the outer membrane first, which could be a significant and

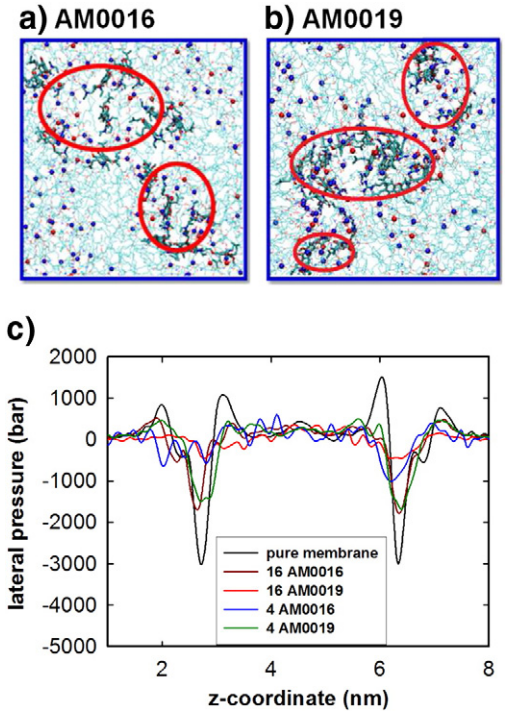

Fig. 4. (a) Snapshots of AM0016 (a) and AM0019 (b) clusters at high concentrations. Blue and red dots represent the phosphate groups of POPE and POPG, respectively. Red circles indicate clusters. (c) Lateral pressures of the bacterial membrane in the presence of AM0016/AM0019.

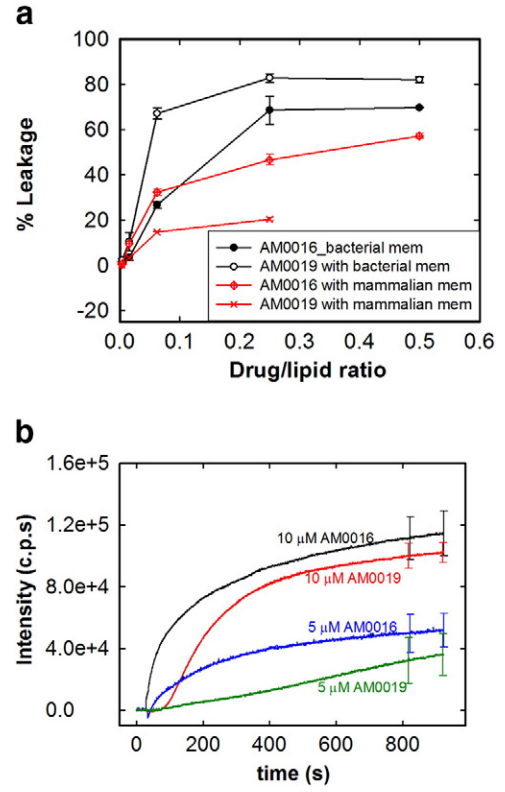

Fig. 5. Dye-leakage experiments of AM0016/AM0019. (a) Percent leakage of calcein from LUV 30 min after addition of AM0016/AM0019 at different drug/lipid ratios using liposome with DOPE/DOPG = 3/1 mimicking the bacterial inner membrane and DOPC/cholesterol = 3/1 mimicking the mammalian membrane. (b) Fluorescence intensity induced by AM0016/AM0019 using living bacterial cells and SYTOX green.

differential barrier. Thus the discrepancy between the dye-leakage experiment and the microbe sterilization assays suggests that the outer membrane servers as a higher diffusion barrier to AM0019 than to AM0016. These differences may arise as AM0019 shows less hydrophobicity due to the presence of the guanidinium group. To verify this, we conducted a SYTOX green leakage experiment using live bacterial cells [44]. The results indeed show that AM0016 induced more membrane perturbations than did AM0019, which confirms that the outer membrane serves as a higher barrier to the inward movement of AM0019 than it does to that of AM0016 (Fig. 5b). The results also suggest that although the rate limiting step of killing of Gram positive bacteria is usually the disruption of the inner membrane, the permeability of a drug across the outer membrane (e.g., the thick peptidoglycan layer) can also affect its antimicrobial activity, at least quantitatively. In a control experiment using Gram negative strains (Table 1), both AM0016 and AM0019 showed no activity because of the barrier to permeation presented by the LPS layer of the Gram negative strains, which further confirms the role of the outer membrane in antimicrobial activity.

Besides activity, another important issue in the drug development is toxicity. In order to examine the toxicity of AM0016 and AM0019, we performed calcein leakage experiments using a LUV (DOPC/cholesterol = 3/1) to mimic the mammalian membrane. Figs. 5a and S7 showed that both AM0016 and AM0019 induce lower leakage of mammalian membrane than bacterial membrane. To understand membrane selectivity at molecular level, we performed MD simulations using different number of AM0016 with model mammalian and bacterial membranes, corresponding to different drug/lipid ratios. Fig. S8 shows that AM0016 adsorbs on the bacterial membrane much faster than on the mammalian membrane, as a result of favourable electrostatic interactions. Moreover, AM0016 was found to penetrate more into the bacterial membrane than into the mammalian membrane, as revealed by the distance between AM0016 and the bilayer centre. We then varied the number of drug/lipid ratio in the MD simulations and used the electrostatic potential to characterize the surface concentration of AM0016 on both membranes [45]. As shown in Fig. S9, the bacterial membrane displays a very negative electrostatic surface potential compared with the mammalian membrane, whose electrostatic surface potential is neutral. As more number of AM0016 adsorbed on the membrane surface, the electrostatic surface potential shifts to more positive values. Fig. S9 clearly showed that even after the adsorption of 9 AM0016 molecules, the bacterial membrane still displays patches with negative potential, while the surface potential of mammalian membrane is saturated after adsorption of 4 AM0016 molecules. This suggested much higher surface concentrations of AM0016 on the bacterial membrane than on the mammalian membrane, which may be responsible for its selectivity towards the bacterial membrane.

We also performed hemolysis test for both AM0016 and AM0019 using red blood cells (HC50) and cytotoxicity test using lactate dehydrogenase (LDH) release assays using human corneal fibroblast cells. The results showed that both AM0016 and AM0019 displayed much higher HC50 values than their respective MIC values, suggesting that selectivity of the two compounds were towards the bacterial membrane. Furthermore, toxic levels of AM0016 and AM0019 based on LDH release assays also revealed a higher lethal dosage of AM0016 and AM0019 than the MIC values, consistent with the simulation results, the calcein leakage and the hemolysis data. On the other hand, compared to AM0016, AM0019 is less toxic and exhibits higher hemolysis values (HC50) and lethal dosages (Table 2), as a result of the reduced hydrophobicity of the guanidinium group of AM0019 with respect to the diethylamide group of AM0016. The above results suggest that the pharmacophore model proposed here is a useful molecular template for the practical design of membrane active molecules.

Table 2
Lethal dosages of xanthone analogues (μg/mL).

	Description	XAN-016	AM0016	AM0019
[a]HC50	Rabbit blood cell	>200	19.6	62.6
[b]LDH	Human corneal fibroblast cells	ND	5.71	21

[a] Concentration required to kill 50% red blood cells.
[b] Lactate dehydrogenase assay using human corneal fibroblast cells.

3. Discussion

From the above MD results, a three-step action mechanism of the bolaamphiphiles AM0016 and AM0019 can be deduced: adsorption–translocation–disruption. Upon adsorption on to the bacterial inner membrane, the molecule first takes a "U-shaped conformation" with both cationic groups interacting with the charged outer leaflet, perturbing only one extracellular hydrophobic–hydrophilic interface. At low concentrations, the molecules remain there because the free energy barrier is too high for the cationic group to further penetrate into the hydrophobic region of the bacterial membrane. As increasing numbers of molecules get adsorbed onto the membrane, the outer leaflet of the inner membrane is gradually neutralized, the drug molecules begin to experience the electrostatic attraction from the inner leaflet and the membrane starts to deform, resulting in a reduction in the free energy barrier for translocation of the molecules. This is followed by a conformational change from the U-shaped conformation to a transmembrane conformation where one of the cationic groups crosses the hydrophobic region to interact with the other charged surface, perturbing both membrane interfaces. It is also possible that some molecules fully translocate across the lipid tail region and adopt U-shaped conformations at the inner leaflet, particularly at high concentrations. When a sufficient number of molecules are in the transmembrane conformation, the membrane undergoes significant deformations and large lipid defects form, leading to the translocation of large numbers of water molecules. Meanwhile, 2-D aggregates begin to form across the membrane and cause a redistribution of the anionic lipids around clusters of the molecules, resulting in changes in the elastic properties of the membrane, ensuing in membrane destabilization.

In the proposed pharmacophore model, a minimum of three fragments are needed: a central hydrophobic core and two cationic terminal groups; each fragment has a particular role. The hydrophobic scaffold plays an important role in partitioning into the bacterial membrane. The MD simulations identify some unique properties that endow alpha-mangostin as an excellent hydrophobic scaffold. Firstly, alpha-mangostin demonstrates enough hydrophobicity to partition into the lipid tail region of the bacterial membrane. Second, even in the transmembrane conformation, AM0016/AM0019 does not achieve a perfect hydrophobic–hydrophilic match with the bacterial membrane due to the presence of the polar groups in the alpha-mangostin scaffold. This results in "disruptive amphiphilicity", which is believed to induce lipid defects [30]. Thirdly, the aromaticity and planarity of the ring structure of the alpha-mangostin molecules enable this scaffold to stack in the lipid tail region of the bacterial membrane, as shown by the 2-D aggregates of AM0016 and AM0019. The 2-D aggregates, together with the cationic groups, further induce membrane deformation and lipid reorganization, forming micro-domains that consist of positively charged AM0016/AM0019 aggregates surrounded by anionic lipids (e.g., POPG). Besides the hydrophobic fragment, the two cationic fragments of AM0016 and AM0019 preferentially interact with the anionic head groups of the bacterial membrane, leading to selectivity towards bacterial membranes. The results of AM0016 and AM0019 suggest that to achieve strong interactions with the anionic head groups, high pKa values, low hydrophobicity and the ability to form multiple hydrogen bonds with the phosphate groups are the important biophysical properties of the cationic fragments. Additionally, other properties of the cationic groups such as the number of positive charges, the shape and size of the cationic groups will likely also modulate the interactions with the anionic head groups of the membrane. There is also the possibility of manipulating the linkers that join the hydrophobic and cationic

moieties of the molecules. We have not explored their variations in this study because the current study is really to demonstrate proof-of-principle; we have minimized the incumbent complexities. However, it is very likely that the lengths and chemical nature of the linkers and the associated flexibility will also influence the barriers that limit the translocation process. In summary, these biophysical parameters provide the basis for further design of new membrane active peptidomimetics.

Considering the fact that the head groups of bacterial membranes are negative while the mammalian membrane is neutral, the pharmacophore model can also achieve selectivity by choosing appropriate cationic fragments that can favourably interact with the anionic head groups of the bacterial membrane via electrostatic interactions. As exemplified in the MD simulations (Figs. S8 and S9), AM0016 binds to the bacterial membrane with faster kinetics and higher affinities than to the mammalian membrane. As a result, AM0016 can accumulate up to a much higher surface concentration on the bacterial membrane than on the mammalian membrane, achieving the selectivity, which is consistent with the interfacial model [30]. The selective interaction of the pharmacophore model to the bacterial membrane was supported by the results of calcein leakage, hemolysis and LDH release assays (Table 2). Moreover, we have shown that topical application of AM0016 has no obvious toxicity to the eyes of mouse and rabbit and does not interfere with wound healing [25]. Altogether, these data demonstrate that the potential of the pharmacophore model with bolaamphiphilic structure can be further optimized into new peptidomimetics with potential clinical applications, at least for topical applications.

Finally, although the action mechanism of the pharmacophore model is exemplified using mangostin analogues AM0016 and AM0019, the choice of the hydrophobic scaffold is not limited to alpha-mangostin. In principle, any hydrophobic molecule with affinity for the lipid tails can be a possible candidate as the hydrophobic scaffold. Indeed, different groups have used different hydrophobic scaffolds to design bolaamphiphilic antimicrobials. Fig. S10 shows the structure of some other membrane active antimicrobials: XF-73 (in phase I clinical trials) [20], brilacidin (in phase II clinical trials) [46,47] and LTX-109 (in phase II clinical trials) [21], mPE [48] and BPMTAs [23], all have a bola-like structure with a central hydrophobic core and two cationic arms, suggesting a mode of action similar to that of AM0016/AM0019, particularly at high concentrations. In addition, the pharmacophore model can be further extended by optimizing each fragment or even by adding additional cationic groups. For example, CSA-13 [49] appears to be a variation of our model in which the central hydrophobic core is replaced by sterol decorated with more than two cationic groups. Finally, toxicity and activity correlate with each other; thus in order to achieve high selectivity one needs to balance these two factors. For example, mammalian membranes often consist of zitterionic lipids with a large content of cholesterol. This suggests that design strategies could benefit from minimizing the affinity of the scaffold with cholesterol moieties.

4. Conclusion

In summary, we demonstrated a simple and yet generalizable pharmacophore model with its detailed mode of action for the ab initio design of membrane active molecules against Gram positive pathogens. The bola-like structure of the pharmacophore model consists of one hydrophobic scaffold and two cationic terminal groups, which were designed to complementarily interact with the lipid tails and the head groups of the bacterial membrane, respectively. Combining MD simulations, biophysical and microbiological experiments to investigate two derivatives of the pharmacophore model, we find compelling evidence supporting the proposed mode of action. Although the safety of the two model compounds needs additional examinations, the approach employed and the pharmacophore model proposed in this study demonstrated the potential for further development of compounds with improved selectivity. Further improvements are currently being carried out to optimize each fragment of the pharmacophore model in order to design better antimicrobials with lower toxicity [50].

5. Methods

5.1. Molecular dynamics simulations

The main lipids of bacterial membrane are POPE and POPG. To have a general model for the bacterial membrane, we employ a mixture of POPE and POPG at a ratio of 3/1 to represent the bacterial membrane, which has been used extensively in other simulation and experimental studies [51–54]. The membrane patch with 72 lipid molecules was used in umbrella sampling molecular dynamics (MD) simulations. The Gromos53a6 force field [55] was used in all the MD simulations. ATB [56] was used to construct the topology of the drug molecules. The translocation free energies of a molecule across the bacterial membrane were calculated from umbrella sampling and weighted histogram analysis method (WHAM) [34,57] using the GROMACS 4.5 package [58]. Due to the introduction of biased potential along the chosen reaction coordinate, umbrella sampling simulations can significantly enhance the phase space sampling. The post-processing algorithm WHAM, which is based on analysis of the data from all the intermediate states at once, reduces the number of cycles and grantees efficiency, demonstrating advantages over other methods such as multiple histogram reweighting method by Ferrenberg and Swendsen [59]. In the simulations, each umbrella window runs for at least 200 ns (Table S1). To understand the membrane affinities of different hydrophobic scaffolds, we also performed a series of conventional molecular dynamics (Table S2). The surface potential of the model membranes was calculated used the APBS plugin of PYMOL [60,61]. In order to study the aggregation of AM0016/AM0019 on the mechanical properties of the membrane, we calculated the pressure field of the bacterial membrane using a customized version of GROMACS [62]. The details of the parameters used in the simulations can be found in the supplementary materials.

5.2. Experimental methods

5.2.1. Susceptibility testing

Susceptibility testing of XAN-016, AM0016 and AM0019 was performed using the broth macro-dilution method in Mueller Hinton Broth (MHB) following Clinical and Laboratory Standards Institute (CLSI) guidelines. Both compounds were first dissolved in *N,N*-dimethylformamide (DMF) and the stock solutions of 1000 μg/mL were prepared. Serial two-fold dilutions of the compounds were then prepared in MHB, Cation Adjusted in test tubes. The concentration of the above-mentioned inoculum suspension was adjusted in MHB until each tube contained approximately 5×10^5 Colony Forming Units (CFU)/mL and incubated at 35 °C for 20 to 22 h. The bacteria used in this study were MRSA DM21455, MRSA 9808R, BC 11778 and Clinical isolates *S. aureus* DM4001. The inoculum suspension was made from isolated colonies selected from an 18- to 20-hour Tryptic Soy Agar (TSA) plate using the direct colony suspension method as prescribed by the CLSI standard.

5.2.2. Hemolysis

Hemolysis was determined as described previously [24,50]. All procedures for isolating blood from New Zealand white rabbits were approved by IACUC Singhealth and performed according to the standards of the Association for the Research in Vision and Ophthalmology.

5.2.3. In vitro cytotoxicity study using lactate dehydrogenase assay

The cytotoxicity of individual compounds screened was determined by the lactate dehydrogenase (LDH) assay. In brief, human corneal fibroblast cells were plated at a density of 10,000 cells per well in a 96-well opaque white plate (SPL Life Sciences Inc). Test compounds of various concentrations and controls were added to appropriate wells

such that the final volume is 100 μL in each well. After 4 h of exposure to the test compounds, the plates were removed from 37 °C incubator and equilibrated to 22 °C for 30 min. One hundred microliters of Cyto-TOX One reagent (Promega Inc. USA) was added to each well and the LDH assay was performed according to the manufacturer's instructions. Fluorescence was assessed at an excitation wavelength of 560 nm and an emission wavelength of 590 nm using a micro-plate reader (Tecan Infinite 200 Pro). The cells exposed to 1% Triton X-100 were used as a positive control and treated as maximum releasing of LDH. The percent specific cytotoxicity of each compound was determined using the formula below:

$$\%\ \text{Cytotoxicity} = \left[\left(I_{\text{experiments}}\right) - \left(I_{\text{negative controls}}\right)\right] / \left[\left(I_{\text{positive controls}}\right) - \left(I_{\text{negative controls}}\right)\right] \times 100$$

where I = intensity measured.

5.2.4. SYTOX green membrane permeabilization assay

The protocol was modified based on the method of Rathinakumar et al. [44] and has been reported [25]. Briefly, overnight a culture of clinical isolate *S. aureus* DM4001 (source: eyes) was harvested at exponential phase. Bacteria were then washed at least 3 times and suspended in 20 mM PBS until OD620 (optical density at 620 nm) of 0.09 was obtained. The bacterial suspension was then incubated with 3 μM SYTOX Green (Invitrogen) in dark conditions for 5 min. Then, the mixture was transferred to a stirring cuvette and the fluorescence emission was monitored using an excitation wavelength of 504 nm and an emission wavelength of 523 nm until the signal was stabilized. Desired concentration of AM0016 and AM0019 was then added and the fluorescence change was measured and recorded. Both compounds were dissolved in DMF and the final % of DMF in the culture was <0.1%. 0.1% DMF had negligible effect on the SYTOX Green fluorescence intensity. Experiments were repeated at least two times and were reproducible. Data from one experiment is presented.

5.2.5. Calcein-loaded LUV leakage study

The release of calcein from the large unilamellar vesicles (LUVs) was studied as previously reported [24]. In brief, the lipids (DOPE/DOPG = 75/25 to mimic bacterial membrane and DOPC/cholesterol = 75/25 to mimic mammalian membrane) were dissolved in methanol/chloroform (1:2, by volume) and were dried gently using a constant stream of nitrogen gas until a thin lipid film was formed. The film was completely dried by placing the film under vacuum for at least 2 h. 80 mM calcein solution was prepared by suspending calcein powder (Sigma Aldrich) in HEPES buffer (50 mM HEPES, 100 mM NaCl, 0.3 mM EDTA, pH 7.4). NaOH solution was added until all calcein suspension was dissolved. Then, the pH of the calcein solution was adjusted to pH 7.4 by adding HCl slowly. Then, the dried lipid film was hydrated using the calcein solution prepared) to obtain a final lipid concentration of 30 mM. The hydrated lipids were freeze-thawed in liquid nitrogen and warm water for 7 cycles. 100 nm homogenous LUVs were then prepared by using an extruder with a polycarbonate membrane (Whatman, pore size 100 nm). The extrusion was done for at least 10 cycles. Sephadex G-50 was used to purify the calcein-loaded LUVs from the free calcein. The concentration of calcein loaded LUVs was determined using total phosphorus determination assay. An aliquot of the LUV suspension was added into a stirred cuvette at various concentrations of AM0016 and AM0019 solution in DMF to obtain the desired compounds to lipid ratios of 1/2, 1/4, 1/16, 1/64, and 1/256. The final concentration of lipid was 50 μM and the final percentage of DMF is <0.2%. Complete leakage was assumed by adding 2% Triton X-100. Control experiment using 0.2% of DMF showed that leakage of calcein from the LUVs was negligible. The calcein released was monitored using a Photon Technology International Model 814 fluorescence spectrophotometer at an excitation wavelength of 490 nm and an emission wavelength of 520 nm. Percentage of leakage (%L) was calculated with %L = [(It − I0) / (I∞ − I0)] × 100], where I0 and It are intensity before and after addition of AM0016 or AM0019 respectively and I∞ is the intensity after the addition of 2% triton X-100.

5.2.6. Chemical synthesis

The details of the chemical synthesis can be found in supplementary materials.

Transparency document

The Transparency document associated with this article can be found, in the online version.

Acknowledgement

This work is supported by funding from ETPL/10-S10FSH-008, NMRC BNIG13nov015, CBRG14may012, TCR/002-SERI/2008/R618 and SHF/FG603S/2013, FG538P/2013, Singapore. The authors thank Alan Mark for helpful discussions. The authors also thank BII, ACRC (A*STAR Computational Resource Center) and CSC (IT Center for Science for computational resources) in Finland for providing the computational facilities.

Appendix A. Supplementary data

Supplementary data to this article can be found online at http://dx.doi.org/10.1016/j.bbamem.2015.01.001.

References

[1] D.I. Andersson, D. Hughes, Antibiotic resistance and its cost: is it possible to reverse resistance? Nat. Rev. Microbiol. 8 (2010) 260–271.
[2] D.M. Sievert, P. Ricks, J.R. Edwards, A. Schneider, J. Patel, A. Srinivasan, A. Kallen, B. Limbago, S. Fridkin, N. Natl Healthcare Safety, N.F. Participating, Antimicrobial-resistant pathogens associated with healthcare-associated infections: summary of data reported to the National Healthcare Safety Network at the Centers for Disease Control and Prevention, 2009–2010, Infect. Control Hosp. Epidemiol. 34 (2013) 1–14.
[3] C.I. Montero, F. Stock, P.R. Murray, Mechanisms of resistance to daptomycin in *Enterococcus faecium*, Antimicrob. Agents Chemother. 52 (2008) 1167–1170.
[4] P. Courvalin, Vancomycin resistance in Gram-positive cocci, Clin. Infect. Dis. 42 (2006) S25–S34.
[5] A.I. Hidron, Jonathan R. Edwards, Jean Patel, Teresa C. Horan, Dawn M. Sievert, Daniel A. Pollock, Scott K. Fridkin, N.H.S.N. Team, P.N.H.S.N. Facilities, NHSN annual update: Antimicrobial-resistant pathogens associated with healthcare-associated infections: annual summary of data reported to the National Healthcare Safety Network at the Centers for Disease Control and Prevention, 2006–2007, Infect. Control Hosp. Epidemiol. 29 (2008) 996–1011.
[6] J.G. Hurdle, A.J. O'Neill, I. Chopra, R.E. Lee, Targeting bacterial membrane function: an underexploited mechanism for treating persistent infections, Nat. Rev. Microbiol. 9 (2011) 62–75.
[7] R.E.W. Hancock, H.G. Sahl, Nat. Biotechnol. 24 (2006) 1551.
[8] C.D. Fjell, J.A. Hiss, R.E.W. Hancock, G. Schneider, Designing antimicrobial peptides: form follows function, Nat. Rev. Drug Discov. 11 (2012) 37–51.
[9] H.D. Thaker, A. Som, F. Ayaz, D. Lui, W. Pan, R.W. Scott, J. Anguita, G.N. Tew, Synthetic mimics of antimicrobial peptides with immunomodulatory responses, J. Am. Chem. Soc. 134 (2012) 11088–11091.
[10] K. Lienkamp, A. Madkour, G. Tew, Antibacterial peptidomimetics: polymeric synthetic mimics of antimicrobial peptides, in: A. Abe, H.-H. Kausch, M. Möller, H. Pasch (Eds.), Polymer Composites – Polyolefin Fractionation – Polymeric Peptidomimetics – Collagens, vol. 251, Springer Berlin Heidelberg, 2013, pp. 141–172.
[11] K. Lewis, Platforms for antibiotic discovery, Nat. Rev. Drug Discov. 12 (2013) 371–387.
[12] E. Matyus, C. Kandt, D.P. Tieleman, Computer simulation of antimicrobial peptides, Curr. Med. Chem. 14 (2007) 2789–2798.
[13] Y. Shai, Z. Oren, From "carpet" mechanism to de-novo designed diastereomeric cell-selective antimicrobial peptides, Peptides 22 (2001) 1629–1641.
[14] H. Leontiadou, A.E. Mark, S.J. Marrink, Antimicrobial peptides in action, J. Am. Chem. Soc. 128 (2006) 12156–12161.
[15] P.J. Bond, D.L. Parton, J.F. Clark, M.S.P. Sansom, Coarse-Grained Simulations of the Membrane-Active Antimicrobial Peptide Maculatin 1.1, Biophys. J., 95 3802-3815
[16] D.B. Kitchen, H. Decornez, J.R. Furr, J. Bajorath, Docking and scoring in virtual screening for drug discovery: methods and applications, Nat. Rev. Drug Discov. 3 (2004) 935–949.

[17] G.N. Tew, R.W. Scott, M.L. Klein, W.F. DeGrado, De novo design of antimicrobial polymers, foldamers, and small molecules: from discovery to practical applications, Acc. Chem. Res. 43 (2009) 30–39.
[18] M. Stark, L.-P. Liu, C.M. Deber, Cationic hydrophobic peptides with antimicrobial activity, Antimicrob. Agents Chemother. 46 (2002) 3585–3590.
[19] L.M. Yin, M.A. Edwards, J. Li, C.M. Yip, C.M. Deber, Roles of hydrophobicity and charge distribution of cationic antimicrobial peptides in peptide–membrane interactions, J. Biol. Chem. 287 (2012) 7738–7745.
[20] N. Ooi, K. Miller, J. Hobbs, W. Rhys-Williams, W. Love, I. Chopra, XF-73, a novel antistaphylococcal membrane-active agent with rapid bactericidal activity, J. Antimicrob. Chemother. 64 (2009) 735–740.
[21] J. Isaksson, B.O. Brandsdal, M. Engqvist, G.E. Flaten, J.S.M. Svendsen, W. Stensen, A synthetic antimicrobial peptidomimetic (LTX 109): stereochemical impact on membrane disruption, J. Med. Chem. 54 (2011) 5786–5795.
[22] R.F. Epand, J.E. Pollard, J.O. Wright, P.B. Savage, R.M. Epand, Depolarization, bacterial membrane composition, and the antimicrobial action of ceragenins, Antimicrob. Agents Chemother. 54 (2010) 3708–3713.
[23] S.K. Vooturi, M.B. Dewal, S.M. Firestine, Examination of a synthetic benzophenone membrane-targeted antibiotic, Org. Biomol. Chem. 9 (2011) 6367–6372.
[24] J.-J. Koh, S. Qiu, H. Zou, R. Lakshminarayanan, J. Li, X. Zhou, C. Tang, P. Saraswathi, C. Verma, D.T.H. Tan, A.L. Tan, S. Liu, R.W. Beuerman, Rapid bactericidal action of alpha-mangostin against MRSA as an outcome of membrane targeting, Biochim. Biophys. Acta Biomembr. 1828 (2013) 834–844.
[25] H. Zou, J.-J. Koh, J. Li, S. Qiu, T.T. Aung, H. Lin, R. Lakshminarayanan, X. Dai, C. Tang, F.H. Lim, L. Zhou, A.L. Tan, C. Verma, D.T.H. Tan, H.S.O. Chan, P. Saraswathi, D. Cao, S. Liu, R.W. Beuerman, Design and synthesis of amphiphilic xanthone-based, membrane-targeting antimicrobials with improved membrane selectivity, J. Med. Chem. 56 (2013) 2359–2373.
[26] H.M. Kulkarni, C.V.B. Swamy, M.V. Jagannadham, Molecular characterization and functional analysis of outer membrane vesicles from the Antarctic bacterium *Pseudomonas syringae* suggest a possible response to environmental conditions, J. Proteome Res. 13 (2014) 1345–1358.
[27] N. Papo, Y. Shai, A molecular mechanism for lipopolysaccharide protection of Gram-negative bacteria from antimicrobial peptides, J. Biol. Chem. 280 (2005) 10378–10387.
[28] S. Gruenheid, H. Le Moual, Resistance to antimicrobial peptides in Gram-negative bacteria, FEMS Microbiol. Lett. 330 (2012) 81–89.
[29] D. Erlanson, Introduction to fragment-based drug discovery, in: T.G. Davies, M. Hyvönen (Eds.), Fragment-Based Drug Discovery and X-Ray Crystallography, vol. 317, Springer Berlin Heidelberg, 2012, pp. 1–32.
[30] W.C. Wimley, Describing the mechanism of antimicrobial peptide action with the interfacial activity model, ACS Chem. Biol. 5 (2010) 905–917.
[31] H.D. Thaker, A. Cankaya, R.W. Scott, G.N. Tew, Role of amphiphilicity in the design of synthetic mimics of antimicrobial peptides with gram-negative activity, ACS Med. Chem. Lett. 4 (2013) 481–485.
[32] T. Wieprecht, M. Dathe, M. Beyermann, E. Krause, W.L. Maloy, D.L. MacDonald, M. Bienert, Peptide hydrophobicity controls the activity and selectivity of magainin 2 amide in interaction with membranes, Biochemistry 36 (1997) 6124–6132.
[33] S.C. McKarns, C. Hansch, W.S. Caldwell, W.T. Morgan, S.K. Moore, D.J. Doolittle, Correlation between hydrophobicity of short-chain aliphatic alcohols and their ability to alter plasma membrane integrity, Toxicol. Sci. 36 (1997) 62–70.
[34] S. Kumar, J.M. Rosenberg, D. Bouzida, R.H. Swendsen, P.A. Kollman, THE weighted histogram analysis method for free-energy calculations on biomolecules. I. The method, J. Comput. Chem. 13 (1992) 1011–1021.
[35] Y. Yan, T. Lu, J. Huang, Recent advances in the mixed systems of bolaamphiphiles and oppositely charged conventional surfactants, J. Colloid Interface Sci. 337 (2009) 1–10.
[36] K.T. Nguyen, S.V. Le Clair, S. Ye, Z. Chen, Molecular Interactions between magainin 2 and model membranes in situ, J. Phys. Chem. B 113 (2009) 12358–12363.
[37] K. Hall, T.-H. Lee, A.I. Mechler, M.J. Swann, M.-I. Aguilar, Real-time measurement of membrane conformational states induced by antimicrobial peptides: balance between recovery and lysis, Sci. Rep. 4 (2014).
[38] P. Yang, A. Ramamoorthy, Z. Chen, Membrane orientation of MSI-78 measured by sum frequency generation vibrational spectroscopy, Langmuir 27 (2011) 7760–7767.
[39] P.C. Dave, E. Billington, Y.-L. Pan, S.K. Straus, Interaction of alamethicin with ether-linked phospholipid bilayers: oriented circular dichroism, 31P solid-state NMR, and differential scanning calorimetry studies, Biophys. J. 89 (2005) 2434–2442.
[40] M.-T. Lee, F.-Y. Chen, H.W. Huang, Energetics of pore formation induced by membrane active peptides†, Biochemistry 43 (2004) 3590–3599.
[41] P.E.S. Smith, J.R. Brender, U.H.N. Dürr, J. Xu, D.G. Mullen, M.M. Banaszak Holl, A. Ramamoorthy, Solid-state NMR reveals the hydrophobic-core location of poly(amidoamine) dendrimers in biomembranes, J. Am. Chem. Soc. 132 (2010) 8087–8097.
[42] E. Lindahl, O. Edholm, Spatial and energetic–entropic decomposition of surface tension in lipid bilayers from molecular dynamics simulations, J. Chem. Phys. 113 (2000) 3882–3893.
[43] A. Ben-Shaul, In Handbook of Biological Physics, in: R. Lipowsky, E. Sackman (Eds.), 1, Elsevier Science, Amsterdam; New York, 1995, pp. 359–401.
[44] R. Rathinakumar, W.F. Walkenhorst, W.C. Wimley, Broad-spectrum antimicrobial peptides by rational combinatorial design and high-throughput screening: the importance of interfacial activity, J. Am. Chem. Soc. 131 (2009) 7609–7617.
[45] J. Li, S. Liu, R. Lakshminarayanan, Y. Bai, K. Pervushin, C. Verma, R.W. Beuerman, Molecular simulations suggest how a branched antimicrobial peptide perturbs a bacterial membrane and enhances permeability, Biochim. Biophys. Acta Biomembr. 1828 (2013) 1112–1121.
[46] B. Mensa, G.L. Howell, R. Scott, W.F. DeGrado, Comparative mechanistic studies of brilacidin, daptomycin and the antimicrobial peptide LL16, Antimicrob. Agents Chemother. 58 (2014) 5136–5145.
[47] S. Choi, A. Isaacs, D. Clements, D. Liu, H. Kim, R.W. Scott, J.D. Winkler, W.F. DeGrado, De novo design and in vivo activity of conformationally restrained antimicrobial arylamide foldamers, Proc. Natl. Acad. Sci. 106 (2009) 6968–6973.
[48] K. Nüsslein, L. Arnt, J. Rennie, C. Owens, G.N. Tew, Broad-spectrum antibacterial activity by a novel abiogenic peptide mimic, Microbiology 152 (2006) 1913–1918.
[49] J.N. Chin, M.J. Rybak, C.M. Cheung, P.B. Savage, Antimicrobial activities of ceragenins against clinical isolates of resistant *Staphylococcus aureus*, Antimicrob. Agents Chemother. 51 (2007) 1268–1273.
[50] J.-J. Koh, S. Lin, T.T. Aung, F. Lim, H. Zou, Y. Bai, J. Li, H. Lin, L.M. Pang, W.L. Koh, S.M. Salleh, R. Lakshminarayanan, L. Zhou, S. Qiu, K. Pervushin, C. Verma, D.T.H. Tan, D. Cao, S. Liu, R.W. Beuerman, Amino acid modified xanthone derivatives: novel, highly promising membrane-active antimicrobials for multidrug-resistant gram-positive bacterial infections, J. Med. Chem. (2014). http://dx.doi.org/10.1021/jm501285x.
[51] W. Zhao, T. Róg, A.A. Gurtovenko, I. Vattulainen, M. Karttunen, Role of phosphatidylglycerols in the stability of bacterial membranes, Biochimie 90 (2008) 930–938.
[52] Y.S. Tu, M. Lv, P. Xiu, T. Huynh, M. Zhang, M. Castelli, Z.R. Liu, Q. Huang, C.H. Fan, H.P. Fang, R.H. Zhou, Destructive extraction of phospholipids from *Escherichia coli* membranes by graphene nanosheets, Nat. Nanotechnol. 8 (2013) 594–601.
[53] A. Khalfa, M. Tarek, On the antibacterial action of cyclic peptides: insights from coarse-grained MD simulations, J. Phys. Chem. B 114 (2010) 2676–2684.
[54] J. Blazyk, R. Wiegand, J. Klein, J. Hammer, R.M. Epand, R.F. Epand, W.L. Maloy, U.P. Kari, A novel linear amphipathic β-sheet cationic antimicrobial peptide with enhanced selectivity for bacterial lipids, J. Biol. Chem. 276 (2001) 27899–27906.
[55] A. Kukol, Lipid models for united-atom molecular dynamics simulations of proteins, J. Chem. Theory Comput. 5 (2009) 615–626.
[56] A.K. Malde, L. Zuo, M. Breeze, M. Stroet, D. Poger, P.C. Nair, C. Oostenbrink, A.E. Mark, An automated force field topology builder (ATB) and repository: version 1.0, J. Chem. Theory Comput. 7 (2011) 4026–4037.
[57] J.S. Hub, B.L. de Groot, D. van der Spoel, g_wham—a free weighted histogram analysis implementation including robust error and autocorrelation estimates, J. Chem. Theory Comput. 6 (2010) 3713–3720.
[58] P. Bjelkmar, P. Larsson, M.A. Cuendet, B. Hess, E. Lindahl, Implementation of the CHARMM force field in GROMACS: analysis of protein stability effects from correction maps, virtual interaction sites, and water models, J. Chem. Theory Comput. 6 (2010) 459–466.
[59] A. Ferrenberg, R. Swendsen, Optimized Monte Carlo data analysis, Phys. Rev. Lett. 63 (1989).
[60] N.A. Baker, D. Sept, S. Joseph, M.J. Holst, J.A. McCammon, Electrostatics of nanosystems: application to microtubules and the ribosome, Proc. Natl. Acad. Sci. 98 (2001) 10037–10041.
[61] T.J. Dolinsky, P. Czodrowski, H. Li, J.E. Nielsen, J.H. Jensen, G. Klebe, N.A. Baker, PDB2PQR: expanding and upgrading automated preparation of biomolecular structures for molecular simulations, Nucleic Acids Res. 35 (2007) W522–W525.
[62] O.H.S. Ollila, H.J. Risselada, M. Louhivuori, E. Lindahl, I. Vattulainen, S.J. Marrink, 3D pressure field in lipid membranes and membrane–protein complexes, Phys. Rev. Lett. 102 (2009) 078101.